# Nanoconfined Water Dynamics in Multilayer Graphene Nanopores



| | |
|---|---|
| Journal: | *The Journal of Physical Chemistry* |
| Manuscript ID | jp-2020-04897r.R1 |
| Manuscript Type: | Article |
| Date Submitted by the Author: | 16-Jul-2020 |
| Complete List of Authors: | Pan, Junchao; Jiangnan University,<br>Xiao, Senbo; Norges teknisk-naturvitenskapelige universitet, Department of Structural Engineering<br>Zhang, Zhiliang; Norges teknisk-naturvitenskapelige universitet,<br>Wei, Ning; Jiangnan University, School of Mechanical Engineering<br>He, Jianying; Norges teknisk-naturvitenskapelige universitet,<br>Zhao, Junhua; Institute of Structural Mechanics, School of Mechanical Engineering, Jiangnan University, 214122 Wuxi, China |
| | |

# Nanoconfined Water Dynamics in Multilayer Graphene Nanopores

Junchao Pan[1], Senbo Xiao[2], Zhiliang Zhang[2], Ning Wei[1*], Jianying He[2*], Junhua Zhao[1*]

[1]*Jiangsu Key Laboratory of Advanced Food Manufacturing Equipment and Technology, Jiangnan University, 214122 Wuxi, PR China*

[2]*NTNU Nanomechancial Lab, Department of Structural Engineering, Norwegian University of Science and Technology (NTNU), 7491 Trondheim, Norway*

## ABSTRACT

Water dynamics in frictionless carbon nanotubes and across ultrathin graphene nanopores have been extensively studied. In contrast, the fundamental properties of nanoconfined water in multilayer graphene nanopores (MGPNs), namely nanopores with rough inner wall, are yet not explored. In this study, nanoconfined water in MGPNs with diameter $D$ ranging from 0.82 to 3.4 nm were investigated by molecular dynamic simulations, providing key dynamics parameters including diffusion coefficient, friction coefficient and shear viscosity. The confinement effect of MGPNs was fully revealed, which indicated a critical pore diameter ($D_c$) of 1.36 nm determining internal water structure and dynamics. Confined water in MGPNs with diameter smaller than or equal to $D_c$ exhibited layer structure and abnormal diffusion. For better understanding water dynamics in MGPNs, water flux and flow enhancement factor were characterized. All the calculated structural and dynamics properties of nanoconfined water in MGPNs were also compared with published results obtained from carbon nanotubes with similar sizes, which for the first time unveiled the impact of inner wall topology of nanopore on nanoconfined water. The results of this study thus laid the solid basis of potential

*Corresponding author. Tel/Fax: +86 510 8591 0562
*Email address*: (NW) weining@mail.tsinghua.edu.cn; (JH) jianying.he@ntnu.no; (JZ) junhua.zhao@163.com

applications of MGPNs and other nanopores with rough inner wall in adsorption and separation of complex fluids, DNA sequencing, seawater desalination, and many others.

**Keywords**: Multilayer graphene nanopores, Nanoconfined water, Diffusion coefficient, Shear viscosity, Water dynamics.

## INTRODUCTION

Nanoconfined water refers to the water confined in the nanospace such as carbon nanotubes (CNTs), nanopores and nanochannels, which is ubiquitous in organic and inorganic nanostructures.[1] It is now well accepted that the properties of water in nanoconfinement substantially differ from what is commonly observed in bulk water.[2] Specifically, the dynamics of nanoconfined water has attracted tremendous interests in recent years, owing to the development of water transport in nanochannels and their potential applications in adsorption and separation of complex fluids,[3] water desalination,[4] efficient energy storage in supercapacitors and batteries,[5] and many others.[6-7]

Hitherto, there have been many encouraging studies devoted to nanoconfined water. Bampoulis *et al*.[3] studied the effect of confinement between mica and graphene on the structure and dynamics of alcohol-water mixtures at the molecular level by atomic force microscopy (AFM). They found that the alcohol molecules showed preferential adsorption at the graphene/ice interface, whereas water domains preferred the mica surface. Zhao *et al*.[8] also studied ethanol-water mixtures and the corresponding pure species, confined within slit-shaped graphene nanopores by molecular dynamics (MD) simulations. They observed that a layered structure was formed within the confined spaces and the ethanol-water mixtures showed segregation at larger pores, where ethanol molecules preferentially adsorbed on graphene surfaces. This microphase demixing behavior stemmed from the competitive effect of the solid-fluid and fluid-fluid interactions. Ma *et al*.[9] created three-dimensional (3D) porous graphene hydrogel adsorbents using an environmentally benign and efficient hydrothermal reduction method. They found that water within hydrogels playing a key role in enhancing adsorption performance and the graphene oxide hydrogels exhibiting an excellent adaptability to environmental factors. Li *et al*.[4] reported an efficient (80% under one-sun illumination) and effective (four orders salinity decrement) solar desalination device utilizing foldable graphene

oxide films, with confined two-dimension (2D) water paths. Fumagalli *et al*.[10] performed local capacitance measurements for water confined between two atomically flat walls separated by varied distances down to 1 nanometer (nm). Their experiments revealed the presence of an interfacial water layer with vanishingly small polarization such that its out-of-plane dielectric constant was only 2 approximately.

Despite the significant achievements in the field of the nanoconfined water from aforementioned studies, there are still many challenges in establishing a universal, comprehensive and governing model for the dynamic behaviour of water in nanopore/nanochannel systems.[11] Nanopores and nanochannels are universal structures playing essential roles in both biological systems and artificial materials[12]. Examples like carbon nanotubes (CNTs),[13] porous carbon,[14] metalorganic frameworks (MOFs)[15] and other organic/inorganic nanostructures[16] have been used as the building blocks of nanopores and nanochannels. As the pore size of these nanomaterials decreases to tens or even several nanometers, the surface/interface effect on physical properties of confined water becomes prominent, which can lead to significant non-linearity, non-monotonicity, non-continuity in water properties and other special characteristics.[16] For example, it is highly difficult to clearly distinguish the solid-liquid interface from the bulk region in small nanochannels.[17] A variety of definitions for the effective size of the confined water appear in previous studies.[2] As a result, many dynamic quantities (such as interfacial tension and interfacial energy) related to the interfacial layer[18] cannot be easily defined. What makes it worse is that the density and pressure of nanoconfined water change dramatically at the water-solid interface with thickness of 1 nm, which has been confined by many experiments and simulations.[17]

Given that many studies have demonstrated different structural and dynamical properties of nanoconfined water molecules from bulk water.[19] However, few studies have comprehensively reported dynamic properties of the confined water in multilayer graphene nanopores (MGPNs,

one kind of rough nanochannels, has many potential applications in design of functional membranes[20] and advanced aqueous batteries[21]). At the same time, graphene nanopores (GPNs) are considered as an ultimate inorganic material[22] owing to their excellent mechanical properties, together with great application prospects in water desalination[23] and low-cost/large-scale energy storage,[24] DNA sequencing,[25] separation of gas[26] and liquid phases[27]. Therefore, it is necessary and significant to understand the confinement effect on dynamic properties of water in these MGPNs.

The aim of this work is to explore the dynamics of nanoconfined water in rough nanochannels by thoroughly scrutinizing the properties of water in multilayer graphene nanopores (MGPNs). Atomistic models of confined water in MGPNs with diameters ranging from 0.82 to 3.4 nm were constructed and subjected to large-scale Molecular Dynamics (MD) simulations. Representative atomic models of nanoconfined water in MGPNs ($D$ = 3.4 nm) can be seen in Figure 1. The oxygen, hydrogen and carbon atoms were colored in red, white and gray, respectively. The MGPNs were constructed by overstacking of 10 graphene nanopores at a uniform distance of 0.34 nm. Other details relevant to the simulation protocols were described in Methods. The structural properties of the confined water in MGPNs were studied. The dynamic properties of the confined water were evaluated and compared with the classical Stokes-Einstein relationship. Furthermore, the confinement effect on hydrogen bonds (HBs) among the water molecules, friction coefficient ($\lambda$), water flow enhancement effect ($\varepsilon$), single water molecule transport potentials of mean forces (PMFs) were also characterized.

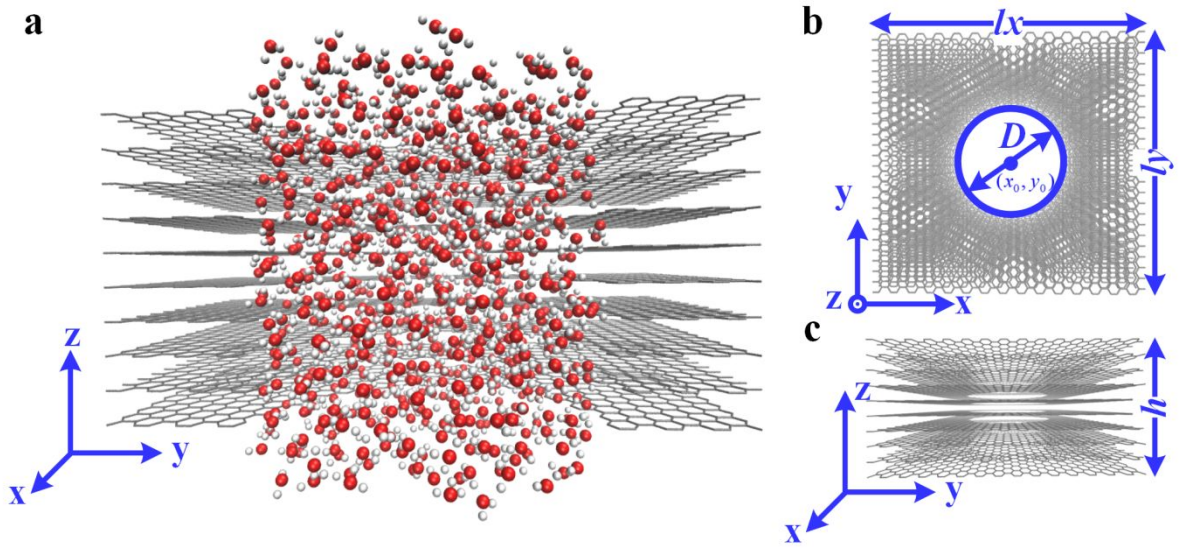


Figure 1. Representative atomic models of nanoconfined water in MGPNs ($D$ = 3.4 nm). (a) Equilibrated nanoconfined water in MGPNs. The oxygen, hydrogen and carbon atoms were colored in red, white and gray, respectively. The MGPNs were constructed by overstacking of 10 graphene nanopores at a uniform distance of 0.34 nm. (b) and (c) were top and side views of the MGPNs. The orientation of the MGPNs were indicated by the coordinate system in each figure.

## METHODS

*Model Construction*. The roughness of MGPNs was created by the stacking edges of GPNs, as a representative atomistic model shown in Figure 1. The axial directions of MGPNs were set along the $z$ direction in all the systems (Figure 1a). In total, eight MGPNs with diameters of $D$ = 0.82, 0.95, 1.1, 1.23, 1.36, 1.63, 2.03, 3.4 nm were constructed in this work, each of which consisting of 10-layer GPNs. The graphene layer distance was uniformly set as 0.34 nm, which is taken as the physical thickness of the graphene membrane.[28-29] The carbon-carbon bond length and bonding angle were 0.142 nm and 120°, respectively, [30] which were constant in all simulations because all the graphene were frozen on the $x$-$y$ plane, as depicted in Figures 1b and 1c.[31] The size of the simulation box was approximately 63.9 × 61.5 × 34 ($l_x$ × $l_y$ × $h$)

nm$^3$ with applied periodic boundary conditions. Water molecules were put into the MGPNs guaranteeing no water clusters nor vacuum regions inside each MGPN.[32] The details of water model and force field parameters are given below. Because of the small internal volume, the addition of one water molecule into the nanopores could results in abrupt rise of internal pressure when the MGPNs were fully filled with water. In this work, no extra water molecule was added into the MGPNs if the average pressure of the confined water showed a change from positive to negative value (see ESI eq S1 for calculation of the internal pressure). The number and the pressure of water molecules in each MGPN were detailed in ESI Figure S1 and Table S1. Snapshots of water molecules confined in different MGPNs after equilibrating simulations were given in ESI Figure S2.

All the MD simulations were performed using the large-scale atomic/molecular massively parallel simulator (LAMMPS).[33] The simple point charge-extended (SPC/E) water model was adopted to combine with parameters from CHARMM force field in all the systems, as previous studies indicated the computational models could accurately predict water properties in confinement.[34-35] The effect of water models on the intercalated water phases was interesting and was discussed in previous work, but not in the scope of the current study.[36] The SHAKE algorithm was used for eliminating high frequency vibrations in the water molecules for enabling simulation time steps of 1 fs.[37] All the carbon atoms of the MGPNs were uncharged and interacted with the oxygen atoms of the water molecules via Lennard-Jones (L-J) potential, which enabled confinement effect to the water in the nanopores.[27] The L-J parameters for the interactions between carbon atoms and the oxygen atoms of water were chosen from the literature, namely $\varepsilon_{CO}$ = 0.093697 Kcal mol$^{-1}$ and $\sigma_{CO}$ = 0.319 nm.[38] Long-range Coulomb interactions between water molecules were treated by particle-particle particle-mesh method (PPPM),[29] with a convergence parameter of $10^{-4}$. The cutoff distances for L-J and Coulomb interactions were set as 1.2 and 1.2 nm, respectively.[28] All the systems were first equilibrated

in the NVT ensemble at a constant temperature of 300 K using the Berendsen thermostat[6] for 40 ns. The coordinates of the water molecules in the MGPNs were collected for analysis in the second half of the equilibration simulation (20ns). The solid-liquid friction coefficient $\lambda$ and the viscosity of the confined water $\eta$ were calculated using the Green-Kubo (GK) relationship.[39] Subsequently, the nanoconfined water was driven by exerting an acceleration $a_{ext}$ after the equilibration simulation, following the previous procedure of realizing Poiseuille flow in MD simulations.[40] To understand the effect of hydrogen bonds (HBs) on the diffusion and the viscosity of the confined water in different MGPNs, the average number of HBs was also monitored. The hydrogen bonding (HB) was defined as the acceptor-donor (O···O) distance less than 0.35 nm and the angle (O-H···O) smaller than 30°.[41] It should be noted that the viscosity, the number of HBs and the diffusion coefficient of the confined water depended on the position of water molecules in nanopores and nanochannels at small sizes.[42] Hence, the average values of the quantities were more meaningful for understanding the nanoconfinement effect of nanopores and nanochannels.[39] For statistical significance, three independent MD simulations were performed for each MD simulation system in this work.

*Calculation of Diffusion Coefficient*. The diffusion dynamics of the confined water was quantified by the diffusion coefficient, which was calculated using the following relationship between the mean squared displacement (MSD) of the center of mass (COM) of the confined water and the exponent of time: [42]

$$\lim_{t\to\infty}\left\langle \left| r(t)-r(0)\right|^2 \right\rangle = \alpha D_{x,y,z} t^n, \quad (1)$$

where $r$ was the coordinate of the COM of the water molecules, $t$ was the time interval, $D_{x,y,z}$ was the average diffusion coefficient in the $x$, $y$ and $z$ direction, $\alpha$ was the dimensional factor which took values of 2, 4, 6 for one-, two-, three-dimensional diffusion, and $n$ was introduced to define the different types of the molecular mobility and the diffusion mechanism, *i.e.*, $n$ = 0.5 (single-file diffusion), $n$ = 1 (the Fickian diffusion), and $n$ = 2 (ballistic diffusion). The

angle bracket "< >" denotes the average values. In this study, the linear section of the MSD of water molecules in the *z* direction was used to compute the average axial diffusion coefficient ($D_z$) (see ESI Figures S6-S7).[43] The MD simulation time was 10 ns, similar to previous works.[44]

*PMF Calculation*. The potential of mean forces (PMFs) of a water molecule migrating along the *z* direction of MGPNs was used to evaluate the mobility of water molecules confined in different MGPNs. The PMFs was calculated using the umbrella sampling method.[45] A restoring harmonic force was applied onto the probing water molecule along the *z* direction of the MGPNs: [45]

$$F_z = K\left(z - z_0\right)M_i / M\,, \tag{2}$$

where $K$ was the harmonic spring constant, $M_i$ was the mass of the $i^{th}$ atom in the target group, $M$ was the total mass of the target group, $z_0$ was the target position for each umbrella sampling window (see ESI Figure S8 and Figure S9).[46] The spring constant $K$ used in the calculation was 1 kcal mol$^{-1}$ Å$^{-2}$. The umbrella sampling window interval was 3 Å covering 90% of the MGPNs' space in the *z* direction. The sampling simulations were performed for 30 ns with a time step of 1 fs, with the trajectories of the last 20 ns collected for analysis for the PMFs using the weighted histogram analysis method (WHAM).[47]

## RESULTS AND DISCUSSION

The confinement has a critical effect on the structure of water molecules, which further defines the dynamics of the confined water.[17] Obviously, water molecules migrating individually or in clusters would result in significantly different diffusion constant. To quantify the variation of water structure confined in different MGPNs, the radial density profile (RDP, as shown in Figure 2a and 2b), the axial density profile (ADP, as shown in Figure 2c and 2d) and the dipole orientation profile (DOP, as shown in Figure 2e and 2f) in different MGPNs were first characterized and compared. The definitions of RDP and ADP were reminiscent to

radial distribution of water here, namely the local water density was normalized by the maximum value found in the system to give a dimensionless value. For the sake of simplicity, "*D*-MGPN" in the following text was used for MGPN with the diameter of *D*.

It is known that water molecules adjacent to a surface exhibit layered structure,[48] which also applies to the inner wall of the MGPNs. Because of the confining space in the MGPNs, the layered structures in each nanopore varied with the diameter *D* of the MGPN. As depicted in Figure 2a, water molecules formed 2-peak structure in MGPNs with diameter smaller than 1.1 nm, meaning only a single-layer of water molecules along the smaller nanopores (see ESI Figure S2). The confined water in the 0.95-MGPN had similar structure as in the 0.82-MGPN, only showing a slight increase in the peak distance of the density thanks to larger diameter. As the diameter increased, there were extra space in the nanopores for accommodating water molecules. As in 1.1- and 1.36-MGPNs (Figure 2a), there thus existed a third density peak in the center region of the nanopores, indicating the emerging of a second-layer water molecules in MGPNs (see ESI Figure S2). As the confined space became larger ($D$>1.23 nm), there were four density peaks in the RDP profiles, with two higher ones adjacent to the wall and two lower one close to the center of the nanopores. These four peaks in the RDP remained as the diameter and the confinement space, became even bigger. There was no further significant density peak observed in the larger MGPNs but a density profile plateau in the center of the nanopores ($D$>1.63 nm). The results indicated that two layers of water molecules can be formed in MGPNs depending on the pore diameter. Because of the limited confinement space, water molecules in smaller MGPNs were involved in layer structuring and were not able to migrate freely without disturbing the integrity of the whole water layers, which may further lead to slow diffusion dynamics.

The confinement space of MGPNs also resulted variation of water density along the axial direction of the nanopores, similar to former studies.[48] The most obvious feature of the axial

water density was the periodic fluctuations of density in the nanopore, with periodicity of the graphene stacking distance of 0.34 nm. As the profiles of ADP shown in Figure 2c, the smaller the nanopore diameter the more prominent the axial water density fluctuation. The most obvious fluctuation in ADP profile was observed inside the 0.82-MGPN, with fluctuation amplitude covering ~40% of the ADP value (Figure 2c, top). In contrast, only marginal fluctuation in the ADP was monitored in the 3.4-MGPN (Figure 2c, bottom), as the inner space in the nanopore render the wall roughness less significant (side views of water molecules shown in ESI Figure S2). Combing with the information in Figure 2a, almost all the water molecules participated in forming layered structure in MGPNs with diameter $D \leq 1.36$ nm were subjected to the nanopore confinement effect from inner wall roughness. The nanoconfined structuring of water molecules and roughness effect were expected to greatly impact water transport, as former studies indicated that structured water molecules could only diffuse in a collective motion.[44]

The structuring of water molecules resulting from nanoconfinement in MGPNs inevitably led to special molecular arrangement and orientation. As each water molecule carrying a dipole, nanoconfinement could also result in unique water electrical properties.[49-50] The net dipole of the water molecules in the MGPNs was calculated, as the total dipole orientation profile (DOP) along the $z$ direction shown in Figure 2e and 2f. Indeed, there was net dipole in the nanopores with diameter $D < 1.36$ nm. In both 0.82-MGPN and 0.95-MGPN, most of water dipoles showed orientation angles $\psi$ in a range of 0 ~ 60° with respect to the nanopore axis (0 ~ 60° in 0.82-MGPN or 120° ~ 180° in 0.95-MGPN). The preference of water dipole orientation decreased as the diameter of the MGPNs increase. In the largest nanopore, 3.4-MGPN, the water molecular dipole angles showed a normal distribution centered at 90° and negligible net dipole in the system (Figure 2e, bottom). The stability of the water dipole orientation in the MGPNs was further tested and confirmed by multiple simulations, as results shown in ESI Figure S4.

The polarization effect of the nanoconfined water in the MGPNs was resulted from the structuring of the water molecules, which could open an avenue for future research on nanoconfined electrical properties of water.[51]

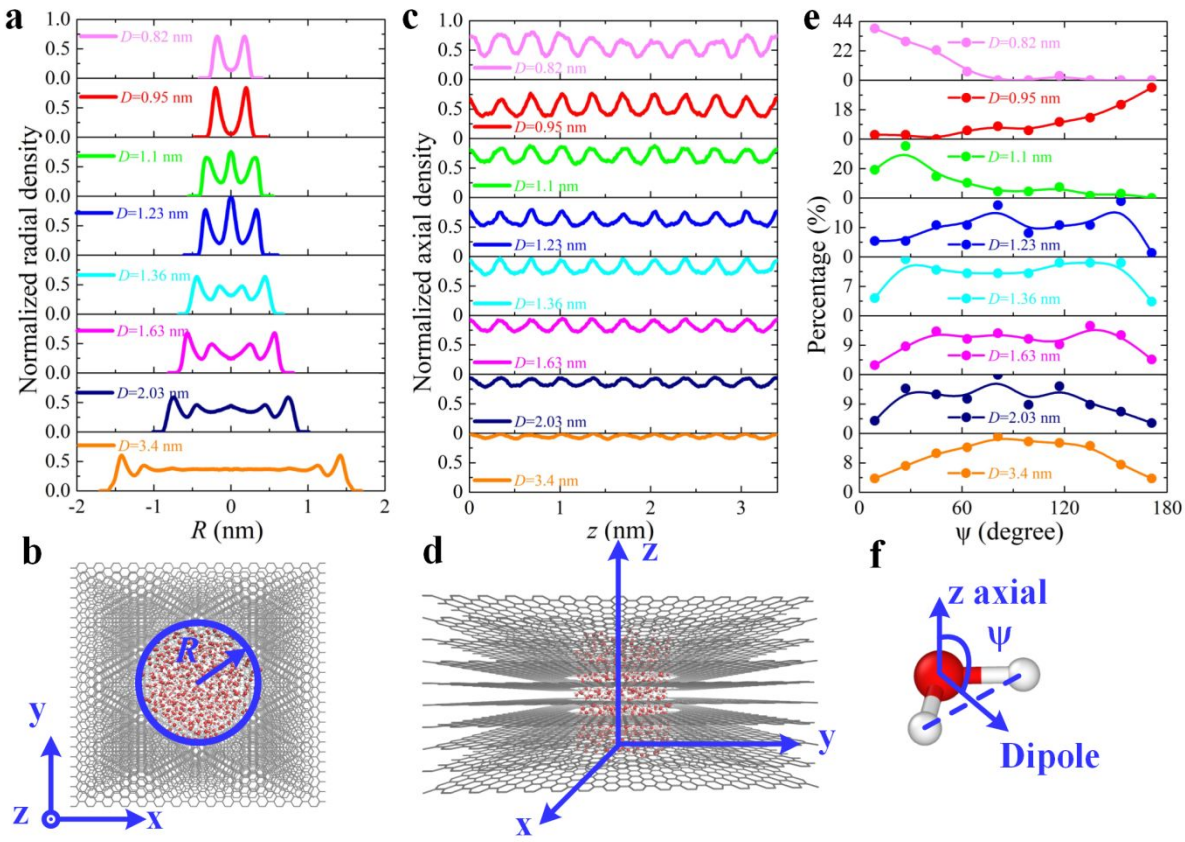


Figure 2. Water structure and dipole orientations in the MGPNs. All the water density profiles are normalized by the maximum values in each system (Here, 1.48295 g cm$^{-3}$ for the radial density, 0.47902 g cm$^{-3}$ for the axial density). (a-b) Radial density profile (RDP) in different MGPNs, and representative schematic of the radial density. (c-d) Axial density profile (ADP), and representative schematic of the axial density; (e-f) Water dipole orientation profile (DOP) in different MGPNs connected with B-Spline,[52] and the definition of the water dipole orientation angle $\psi$.

To further elucidate the effect of confinement on nanoconfined water dynamics in MGPNs, we investigated many dynamic parameters of nanoconfined water. Diffusion is one of the most interesting research topics of nanoconfined water dynamics, which is also highly relevant in

various applications.[42] The diffusion of water molecules along the MGPNs was first quantified for probing the water dynamics in nanopores with rough inner wall. The axial diffusion coefficient $D_z$ of water molecules confined in different MGPNs is shown in Figure 3a, where the color strip represents standard errors by B-Splines fitting.[52] Meanwhile, there was a critical nanopore diameter $D_c$ (Here, $D_c$ was 1.36 nm) for water molecule diffusion in the confining space of the MGPNs. The water diffusion coefficient $D_z$ was close to bulk water if the MGPN diameter $D > D_c$. In contrast, water diffusion $D_z$ deviated substantially in MGPNs with diameter $D \leq D_c$. It should be noted that all the water molecules were involved in the layered structure in the MGPNs with diameter $D \leq D_c$ (Figure 2a). The high diffusivity observed in 0.95-MGPN and 1.36-MGPN thus was resulted from their confined water structure for optimizing water diffusion. The high diffusivity in the two system was also similar to results from previous studies.[36] It was found that 2D diffusivity of water molecules confined in graphene nanogap was significantly higher than in bulk water.[53] Interestingly, there seems to be a similar critical pore diameter (1.36 ~1.63 nm) for water diffusion in carbon nanotubes (CNTs). By comparing results from water diffusion in CNTs with the same diameters and at the same temperature (results of CNTs from Farimani *et al*.[42], Zheng *et al*.[43], Köhler *et al*.[54], Won *et al*.[55]), the $D_z$ of water molecules was also close to bulk water in the CNTs with diameter larger than 1.36 nm, otherwise significantly lower in smaller CNTs (Figure 3a, data points from references). Despite the rougher inner wall surface, water molecules $D_z$ monitored in MGPNs with diameter $D \leq$ 1.36 nm were approximately one order of magnitude higher than in CNTs with the same diameters (Further discussion below).

It is important to clarify whether a nanopore as a whole being an interface or its inner wall being a surface are inner wall to the confined water molecules. As shown in Figure 2a, nanoconfined water molecules presented all layered structure (the nanopore being an interface) or partially structured and partially bulk-like (inner wall of the nanopore being a surface). Thus,

it is necessary to distinguish the two effects in the water axial diffusion coefficient $D_z$, which has been detailed discussed in former studies.[56] As shown in Figure 3a, the dependence of water axial diffusion coefficient $D_z$ on the diameter of MGPNs is non-monotonic, which was an indication of the combined interface and surface effects. It is not the scope of this work to separate these two effects but rather their synergy in the properties of nanoconfined water in MGPNs.

In order to clarify the effect of inner wall roughness on nanoconfined water dynamics in MGPNs, the friction coefficient $\lambda$ of the water-MGPNs interface was calculated in our equilibration simulations following the GK relationship: [57-58]

$$\lambda = \frac{1}{Ak_BT}\int_0^\infty \left\langle F_z(t)F_z(0)\right\rangle dt\,, \tag{3}$$

where $F(t)_z$ was the total forces exerted on the water intercalation from its interaction with MGPNs in the $z$ direction, $k_B$ was the Boltzmann constant ($k_B = 1.38\times10^{-23}$ J K$^{-1}$), $A$ was the surface area, and $T$ was the water temperature. As shown in Figure 3b, the minimum $\lambda$ was found in 1.36-MGPN, corresponding to the highest water diffusion $D_z$ in the same nanopore discussed above. Similar to water diffusion coefficient, $\lambda$ values in MGPNs featured obvious variation if the nanopore diameter $D \leq D_c$. Given that the nanoconfined water molecules in these MGPNs were structured with tailored net dipole orientation (as shown in Figure 2e), which could alter and weaken atomistic interactions between the water molecules and the inner wall of the MGPNs.[40] The friction coefficient $\lambda$ of water in similar sizes of CNTs was compared to the calculated results, as given in Figure 3b. CNTs was known for their frictionless inner wall to water, which resulted in much lower friction coefficients. It should be noted that the wall of CNTs is single-atom layer,[29] while the wall of MGPNs was much thicker. Water molecules thus had much weaker atomistic interactions with CNT than with MGPNs, which could lead to higher preference of water entrance in CNTs. The confinement effect also

strongly influenced the hydrogen bonds (HB) in water, yet another important factor of water dynamics.[42, 59] The average HB numbers $<N_{HB}>$ of the nanoconfined water in different MGPNs were examined, as shown in the inset of Figure 3b. The average HB number per water molecule was reduced to be 1~1.2, much lower than in CNTs[42, 60] and bulk water.[42] The HBs differences of nanoconfined water in MGPNs and CNTs can also help understand the differences of diffusion coefficients.[36]

Besides the diffusion and the friction coefficients, shear viscosity of water in the MGPNs were characterized for better understanding of nanoconfined water dynamics. The shear viscosity $\eta$, including the axial ($\eta_{xz}$) and radial ($\eta_{xy}$) viscosity, calculated by integrating the ACF of pressures in the nanopores using the GK relationship,[61]

$$\eta_{xz} = \frac{V}{k_B T}\int_0^\infty \left\langle P_{xz}(t) P_{xz}(0)\right\rangle dt , \tag{4}$$

$$\eta_{xy} = \frac{V}{k_B T}\int_0^\infty \left\langle P_{xy}(t) P_{xy}(0)\right\rangle dt , \tag{5}$$

where $V$ was the nanopore volume, $P_{xz}$ and $P_{xy}$ were the axial and radial shear pressure respectively. As shown in Figure 3c, the axial viscosity of water in the MGPNs, $\eta_{xz}$, featured an increase pattern with the pore diameter $D$ and again exhibited deviations if the diameter $D \leq D_c$. A cross-sectional averaged effective model of weighted-average viscosity was previously used to describe water shear viscosity in MGPNs accounting for the water-wall interface effect,[62]

$$\eta_{xz}(D) = c\eta_i \frac{A_i(D)}{A_t(D)} + c\eta_B\left[1 - \frac{A_i(D)}{A_t(D)}\right], \tag{6}$$

where $\eta_i$ and $A_i$ were the shear viscosity and the area of the interface region of the structured water, respectively, $A_t$ was the total cross-sectional area, and $c$ was a dimensionless parameter introduced to describe the synergistic effects of these factors. Here, $A_t(D) = \pi(D/2)^2$, $A_i(D) = \pi(D/2)^2 - \pi(D/2 - t_{inter})^2$, and $t_{inter}$ signified the thickness of the annular region adjacent to the

wall of MGPNs. The model accounted for shear viscosity contribution from the interfacial structured water in the interface region ($\eta_i$) and the bulk-like water ($\eta_B$) in the center of large nanopores, and took into account of parameters including the effective size of the confined water,[2, 63] the density of the water, temperature and the size of confinement.[39] As shown in Figure 3c, water shear viscosity in the MGPNs was fitted by eq 6, using formerly reported $\eta_B$ = 0.83 mPa·s,[58] $\eta_i$ = 0.2 mPa·s, $t_{inter}$ = 0.2807 nm and $c$ = 0.2879 ($c$ is within the range of values from previous studies[2]). The calculated results indeed followed the trend predicted by the analytical model. The axial water viscosity $\eta_{xz}$ in all MGPNs was approximately two orders larger than radial viscosity $\eta_{xy}$, which was also similar what was observed in CNT of similar sizes.[54]

It was known that the shear viscosity and the axial diffusion coefficient in nanopores can be described by the Stokes-Einstein relationship:[64] $\eta_{xz}D_z = k_B T/3\pi a$. The constant $a$ in the relationship was the effective atomic diameter, which for water can be considered as the first peak in the radial distribution function (RDF) from the solid surface.[65] The calculated shear viscosity and axial diffusion coefficient of the nanoconfined water in this work followed the Stokes-Einstein relationship in MGPNs of $D > D_c$, which did not hold in MGPNs with diameter $D \le D_c$. In order to quantitatively describe the strong deviation of the key parameter from the Stokes-Einstein relationship in small MGPNs, a refined theoretical model was introduced,

$$D_z = \begin{cases} \omega_1 \dfrac{k_B T \zeta^n}{\pi a \eta_{xz}} & for \quad D < D_c, \quad n = 1 \\ \omega_2 \dfrac{k_B T \zeta^n}{\pi a \eta_{xz}} & for \quad D \ge D_c, \quad n = 0 \end{cases}, \tag{7}$$

where $\zeta^n = (D/D_c)^n$ was used for describing the influence of $D$ on dynamic properties of the confined water, featuring the similar manner of describing the nanochannel thickness effect on the confined liquid in previous study.[39] By taking the critical diameter $D_c$ = 1.36 nm, water effecting diameter $a$ = 0.275 nm (similar to previous studies[66] and RDF as shown in ESI Figure

S3), and fitting parameters of $\omega_1 = 0.06545$ and $\omega_2 = 0.0916$, the results in this work were fitted as shown in Figure 3d. This new refined theoretical model could thus describe this abnormal relationship of water diffusion coefficient and shear viscosity in small MGPNs, with prediction errors smaller than 10% ($D < D_c$) and 20% ($D \geq D_c$, approximately 40% in a previous study[67]). The reliability of the refined model (eq 7) was further tested with water axial diffusion coefficient and shear viscosity obtained at different simulation time of 10 ns, which was confirmed with error of < 15%.

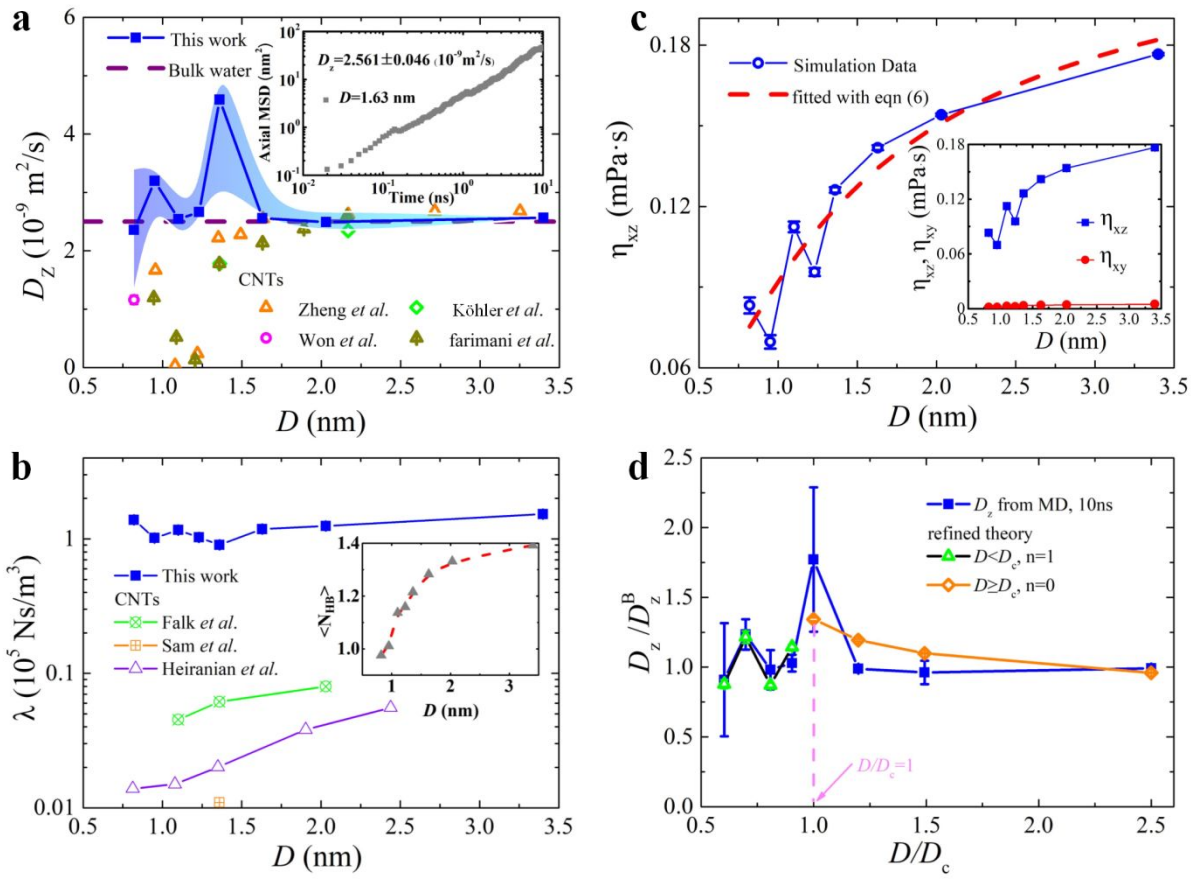


Figure 3. Nanoconfined water properties in MGPNs. (a) Axial diffusion coefficient $D_z$, with color strip represents errors by B-Splines.[52] The inset shows the representative section of the mean squared displacement (MSD) used for calculating $D_z$, with more examples given in ESI Figures S6-S7. The diffusion coefficient of the bulk water $D$B Z= 2.59 × $10^{-9}$ $m^2$ $s^{-1}$ (purple dash line) is given for comparison.[42] Previous reported water axial diffusion coefficient are shown with data adopted from Farimani *et al.*[42], Zheng *et al.*[43], Köhler *et al.*[54], Won *et al.*[55].

(b) Friction coefficients of water molecules in different MGPNs. Former published results of water friction coefficient in CNTs are used for comparison, with data adopted from Falk *et al*.[40], Sam *et al*.[68] and Heiranian *et al*.[29]. The average numbers of HBs per water molecule in each MGPNs are shown as inset. (c) Axial shear viscosity of water $\eta_{xz}$ in different MGPNs, with fitting model given in eq 6 as a red dash line. The inset shows axial ($\eta_{xz}$, blue dotted line) and radial ($\eta_{xy}$, red dotted line) water viscosities. (d) A refined model of $D_z$ and its prediction, with data obtained at simulation time of 10 ns using eq 6.

To better understand the dynamics of nanoconfined water in MGPNs, the potential of mean forces (PMFs) of a single water molecule migrating through the nanopores were calculated (as shown in Figure 4a), which can be taken as the energy landscape of water molecule diffusion. As shown in Figure 4b, the water migration PMFs exhibited a wave-like pattern similar to previous results,[69] indicating water molecules need to cross multiple energy barriers in diffusion in the confinement of MGPNs. The energy barriers in the PMFs profiles were generally higher (Figure 4b) in smaller MGPNs than in larger ones, which can be attributed to the water structures and the nanoconfinement effect. As shown in Figure 2b and 2c, more water molecules were structured, and the fluctuation of internal water density was more severe in smaller MGPNs. Migration of single water molecules in such confined environment would have to first dissociate from and break through the water structure and further experience close contact with the rough inner wall surface. The undulant profiles of the PMFs can be quantitatively summarized by its standard deviation $\sigma$, which can be further correlated with the diameter of the MGPNs $D$ for illustrating nanoconfinement effects. Similar analysis has been applied in previous studies,[55] where the $\sigma$ of PMFs of water migration in CNTs was found to be one order of magnitude larger than the results in this work, as shown in Figure 4c. Such different support the higher water axial diffusion coefficients in MGPNs than in CNTs if the nanopore diameter $D \leq D_c$. Furthermore, the $\sigma$ of PMFs in this work can be fitted by a proposed

model (eq 8) inspired by the double barrier model for the trapping of dihydrofolate reductase (DHFR) and the Eyring's molecular-kinetic theory (MKT) for describing the boundary slip at the liquid-solid interface,[70-71]

$$\sigma = wK_BT\left(\frac{D}{\lambda_d}\right)^h, \tag{8}$$

where $(D/\lambda_d)^h$ was a parameter related to the $\zeta^n$ in eq 7, $\lambda_d$ was the average distance of each energy barrier in the PMF profiles.[71] Here, $\lambda_d$ = 0.34 nm was equal to the separation of graphene layers in this work, and $w$ = 0.3441 and $h$ = -1.311 were fitted parameters using eq 8.

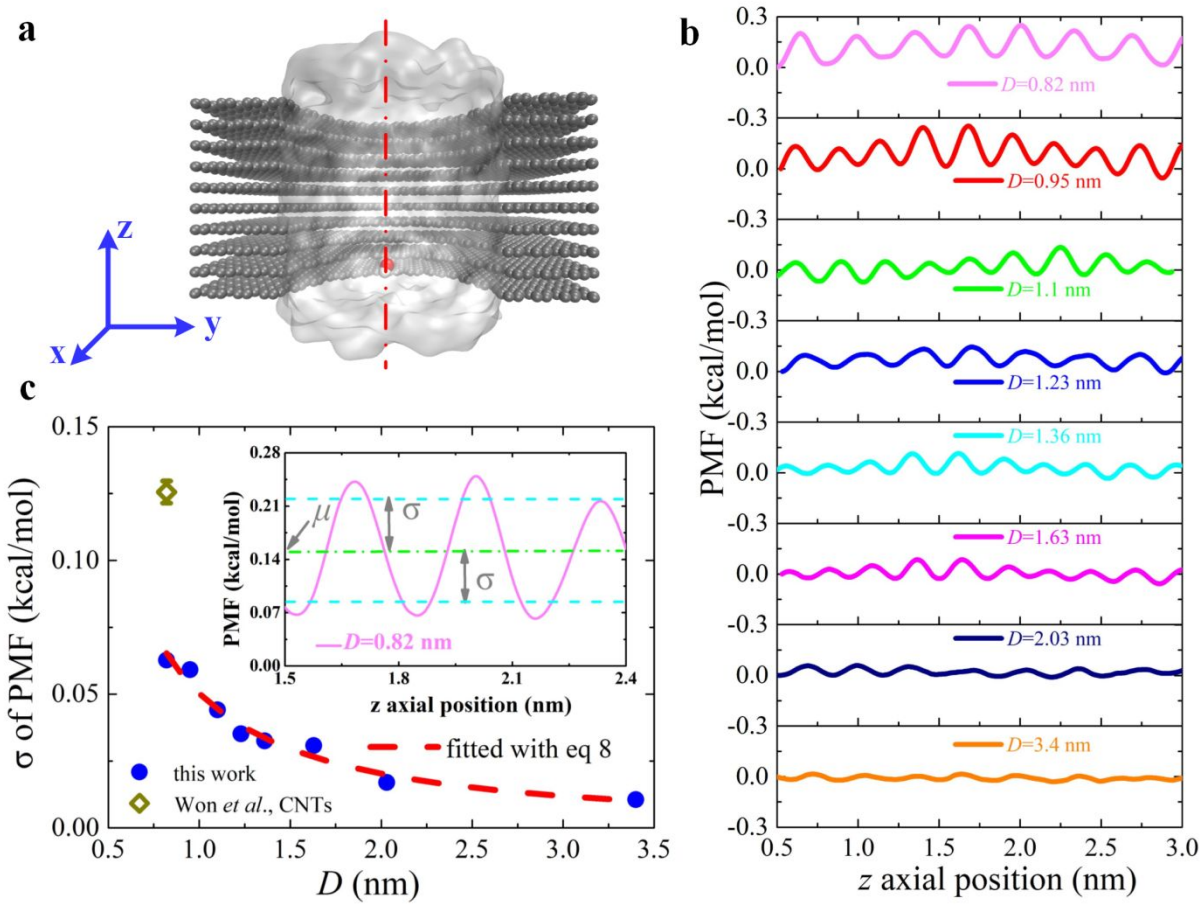


Figure 4. Potential of mean forces (PMFs) of a water molecule migrating through the MGPNs. (a) A typical system snapshot for calculating the PMFs with water migration path indicated by the axis (red dotted line) of the MGPNs. (b) The PMFs of water molecules migration in different MGPNs with their diameter $D$ given as legends. (c) The standard deviation $\sigma$ of water

migration PMFs in MGPNs and CNTs. The results in this work were fitted with the proposed model given in eq 8. The $\sigma$ value of water migration PMFs in CNTs for comparison was monitored in single-walled (6, 6) CNT.[55] The inset illustrated the local fluctuation of the PMF.

As discussed above, water diffusion dynamics in MGPNs with diameter $D \leq D_c$ substantially deviated from the Stokes-Einstein relationship. Such abnormality could be caused by the combined surface and interface effects of the nanopores, namely the synergistic effect of both the inner wall roughness and the degree of confinement in different MGPNs. In order to understand the unique water diffusion dynamics and nanoconfined surface-interface effects on water transport, water molecules in different MGPNs were subject to different pressure gradients $P$ ($P$ = 3, 4, 5, 6 and 7 MPa nm$^{-1}$, with more details given in ESI Figure S5 and ESI Table S2).The pressure driven water flux $Q$ and the flow enhancement factor $\varepsilon$ were then quantified. Briefly, the flux $Q$, $Q = Nm/N_A\rho$, was calculated by counting the number of water molecules ($N$) passing through MGPNs per unit time per unit cross-section area ($m/N_A\rho$, with $m$ being water molecular weight molar mass, $N_A$ the Avogadro number and $\rho$ the water density). The flow enhancement factor $\varepsilon$ was defined as $\varepsilon = Q/Q_{HP}$, where $Q_{HP} = \pi D^4 a_{ext}\rho/128\eta_{xz}$ was the no-slip Hagen–Poiseuille reference flux with acceleration $a_{ext}$ under external driven pressure.[68] The relationship between the external pressure and the acceleration was $P = R/2L\tau$, with $\tau = Nma_{ext}/2\pi RL$. Here, $\rho = Nm/\pi L(D/2)^2$, $m$ = 18 g mol$^{-1}$ and nanopore length $L$ = 3.4 nm.

As shown in Figure 5a, the larger the axial pressure gradient $P$ applied in the confined water in the MGPNs, the larger the flux $Q$. The relationship between the $Q$ and the external $P$ in all systems was almost linear, in agreement with previous studies.[64] At the same time, the larger internal volume (confinement space) also resulted in the larger $Q$ under the same pressure gradient $P$. Strikingly, the flux $Q$ in the 1.36-MGPN was larger than in the 1.63-MGPN, owing to the surface and interface effects discussed above. The flow enhancement factor in the

MGPNs was compared with previous results observed in CNTs of similar sizes, as shown in Figure 5b. The values of $\varepsilon$ in MGPNs were approximately two orders of magnitude lower than in CNTs as the nanopore diameter $D \leq D_c$. Although water molecules $D_z$ monitored in MGPNs with diameter $D \leq D_c$ were approximately one order of magnitude higher than in CNTs with the same diameters in terms of thermal motion (Figure 3a), larger friction coefficient $\lambda$ (Figure 3a) in MGPNs hindered water transport in pressure driven. In other words, both thermal motion and transport of water in pressure driven are affected by the surface-interface effect at nanoscale, but they have no absolute dependence. When the diameter increased and reached the critical value $D_c$, the flow enhancement factor is similar in both nanopore types. Such result further confirmed the importance of the surface and interface effects of the nanochannels to the dynamics of the nanoconfined water as previously reported.[72]

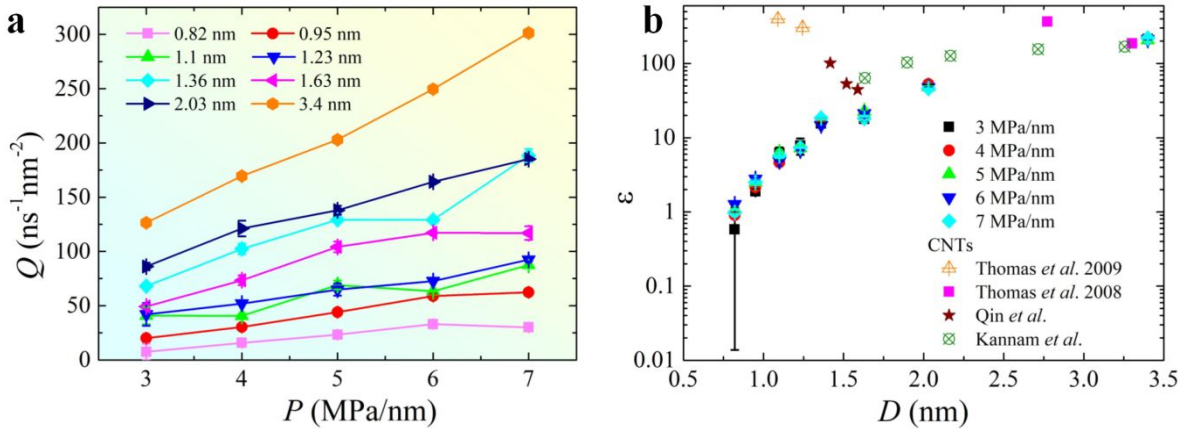


Figure 5. (a) Water flux $Q$ vs. applied pressure gradient $P$ in different MGPNs (the error of three independent MD simulations is within ±5%); (b) the flow enhancement factor $\varepsilon$ against different diameters $D$ using different gradients $P$ (the error is within ±5%). Some other available results of the water confined in CNTs are also presented here, *i.e.* Thomas *et al.*[73], Qin *et al.*[74], Kannam *et al.*[75]

## CONCLUSIONS

To conclude, nanoconfined water was one of the most investigated targets recently, because of their differences from bulk water and great potentials in nanotechnologies. This work devoted to systematically studying the dynamics of nanoconfined water in MGPNs with varied diameter and providing water structural properties resulting from confinement and key dynamics factors including water diffusion coefficient, friction coefficient and shear viscosity. Comparing to CNTs with frictionless inner wall and nanopores in a graphene with ultrathin thickness, the rough inner wall of MGPNs rendered the dynamics of nanoconfined water much more complex. The results showed that there was a critical diameter $D_c$ = 1.36 nm for MGPNs. Water dynamics in MGPNs with diameters smaller than or equal to the critical value became abnormal and could not be described by the well-known Stokes-Einstein relationship. However, the abnormality of water dynamics was comprehended if the water structure in small MGPNs was considered. For MGPNs with diameters smaller than or equal to $D_c$, they served wholly as interfaces to the confined water leading to internal water structuring. In contrast, MGPNs with diameters larger than $D_c$ allowed unstructured water adjacent to nanopore axis, meaning their inner walls served as surfaces to nanoconfined water. Such differences in internal water structures thus further resulted in rougher energy landscape for water transport under driven pressure in smaller MGPNs. Overall, this work scrutinized the crucial dynamics properties of nanoconfined water in MGPNs, namely nanochannels with rough inner wall and its combined effect in nanoconfinement, which could promote the development and applications of MGPNs and similar nanopores areas like seawater desalination, DNA detection, efficient energy storage in supercapacitors and batteries, adsorption/separation of complex fluids, and other related material science and technology.

# CONFLICTS OF INTEREST

The authors declare no competing financial interest.

## Supporting Information

Additional details of the simulation models, snapshots of water molecules confined in different MGPNs under thermodynamic equilibrium states, radial distribution function (RDF) of the confined water, dipole orientation profile (DOP) along the *z*-direction of the confined water in different MGPNs, average velocity $V_{\text{average}}$ of the confined water under different pressure gradients, MSD of water molecules confined in different MGPNs and histograms of configurations


# ACKNOWLEDGEMENTS

We gratefully acknowledge support from the National Natural Science Foundation of China (Grant Nos. 11972171, 11572140 and 11502217), the Natural Science Foundation of Jiangsu Province (Grant Nos. BK20180031), the 111 project (Grant No. B18027), the National First-Class Discipline Program of Food Science and Technology (Grant No. JUFSTR20180205), Primary Research & Development Plan of Jiangsu Province (Grant No. BE2017069), Research Project of State Key Laboratory of Mechanical System and Vibration (Grant No. MSV201909), Science and Technology Plan Project of Wuxi, the Fundamental Research Funds for the Central Universities (Grant Nos. JUSRP11529 and JG2015059), the Project of Jiangsu provincial Six Talent Peaks in Jiangsu Province. The computational resources were provided by the Norwegian Metacenter for Computational Science (NOTUR NN9110 and NN9391K).


# REFERENCES

(1) Raviv, U.; Laurat, P.; Klein, J., Fluidity of Water Confined to Subnanometre Films. *Nature* **2001**, *413*, 51.

(2) Neek-Amal, M.; Peeters, F. M.; Grigorieva, I. V.; Geim, A. K., Commensurability Effects in Viscosity of Nanoconfined Water. *ACS nano* **2016**, *10*, 3685-92.

(3) Bampoulis, P.; Witteveen, J. P.; Kooij, E. S.; Lohse, D.; Poelsema, B.; Zandvliet, H. J., Structure and Dynamics of Confined Alcohol-Water Mixtures. *ACS nano* **2016**, *10*, 6762-8.

(4) Li, X.; Xu, W.; Tang, M.; Zhou, L.; Zhu, B.; Zhu, S.; Zhu, J., Graphene Oxide-Based Efficient and Scalable Solar Desalination under One Sun with a Confined 2d Water Path. *Proceedings of the National Academy of Sciences of the United States of America* **2016**, *113*, 13953-13958.

(5) Yang, X.; Zhu, J.; Qiu, L.; Li, D., Bioinspired Effective Prevention of Restacking in Multilayered Graphene Films: Towards the Next Generation of High-Performance Supercapacitors. *Advanced materials* **2011**, *23*, 2833-8.

(6) Pan, J.; Wei, N.; Zhao, J., Shear Properties of the Liquid Bridge between Two Graphene Films Using a Refined Molecular Kinetics Theory and Molecular Dynamics Simulations. *Mechanics of Materials* **2019**, *137*, 103124.

(7) Pan, J.; Ding, D.; Dong, S.; Liu, Y.; Wei, N.; Zhao, J., A Theoretical Analysis of Peeling Behavior between Nanowires and Substrates in the Ambient Condition with High Relative Humidity. *Mechanics of Materials* **2017**, *114*, 243-253.

(8) Zhao, M.; Yang, X., Segregation Structures and Miscellaneous Diffusions for Ethanol/Water Mixtures in Graphene-Based Nanoscale Pores. *The Journal of Physical Chemistry C* **2015**, *119*, 21664-21673.

(9) Ma, J.; Yang, M.; Yu, F.; Zheng, J., Water-Enhanced Removal of Ciprofloxacin from Water by Porous Graphene Hydrogel. *Sci Rep* **2015**, *5*, 13578.

(10) Fumagalli, L., et al., Anomalously Low Dielectric Constant of Confined Water. *Science* **2018**, *360*, 1339-1342.

(11) Zhu, Z.; Wang, D.; Tian, Y.; Jiang, L., Ion/Molecule Transportation in Nanopores and Nanochannels: From Critical Principles to Diverse Functions. *Journal of the American Chemical Society* **2019**, *141*, 8658−8669.

(12) Zhang, W.; Wei, S.; Wu, Y.; Wang, Y. L.; Zhang, M.; Roy, D.; Wang, H.; Yuan, J.; Zhao, Q., Poly(Ionic Liquid)-Derived Graphitic Nanoporous Carbon Membrane Enables Superior Supercapacitive Energy Storage. *ACS nano* **2019**, *13*, 10261-10271.

(13) Barber, A. H.; Cohen, S. R.; Wagner, H. D., Static and Dynamic Wetting Measurements of Single Carbon Nanotubes. *Physical review letters* **2004**, *92*, 186103.

(14) Futamura, R.; Iiyama, T.; Takasaki, Y.; Gogotsi, Y.; Biggs, M. J.; Salanne, M.; Segalini, J.; Simon, P.; Kaneko, K., Partial Breaking of the Coulombic Ordering of Ionic Liquids Confined in Carbon Nanopores. *Nat Mater* **2017**, *16*, 1225-1232.

(15) Aijaz, A.; Akita, T.; Yang, H.; Xu, Q., From Ionic-Liquid@Metal-Organic Framework Composites to Heteroatom-Decorated Large-Surface Area Carbons: Superior Co2 and H2 Uptake. *Chem Commun (Camb)* **2014**, *50*, 6498-501.

(16) Zhang, X.; Liu, H.; Jiang, L., Wettability and Applications of Nanochannels. *Advanced materials* **2019**, *31*, 1804508.

(17) Brovchenko, I.; Oleinikova, A., *Interfacial and Confined Water*: Amsterdam: Elsevier, 2008.

(18) Gray, C. G.; Gubbins, K. E.; Joslin, C. G., *Theory of Molecular Fluids: Volume 2: Applications*, 2011.

(19) Leoni, F.; Franzese, G., Effects of Confinement between Attractive and Repulsive Walls on the Thermodynamics of an Anomalous Fluid. *Physical Review E* **2016**, *94*, 062604.

(20) Wei, N.; Peng, X.; Xu, Z., Understanding Water Permeation in Graphene Oxide Membranes. *ACS Appl Mater Interfaces* **2014**, *6*, 5877-83.

(21) Chao, D.; Zhou, W.; Xie, F.; Ye, C.; Li, H.; Jaroniec, M.; Qiao, S.-Z., Roadmap for Advanced Aqueous Batteries: From Design of Materials to Applications. *Science Advances* **2020**, *6*, eaba4098.

(22) Král, P., Realistic Cataloguing of Nanopores. *Nature Materials* **2019**, *18*, 99-101.

(23) Cohen-Tanugi, D.; Lin, L. C.; Grossman, J. C., Multilayer Nanoporous Graphene Membranes for Water Desalination. *Nano letters* **2016**, *16*, 1027-33.

(24) Beltrop, K.; Beuker, S.; Heckmann, A.; Winter, M.; Placke, T., Alternative Electrochemical Energy Storage: Potassium-Based Dual-Graphite Batteries. *Energy & Environmental Science* **2017**, *10*, 2090-2094.

(25) Garaj, S.; Hubbard, W.; Reina, A.; Kong, J.; Branton, D.; Golovchenko, J. A., Graphene as a Subnanometre Trans-Electrode Membrane. *Nature* **2010**, *467*, 190-3.

(26) Jiang, D.-e.; Cooper, V. R.; Dai, S., Porous Graphene as the Ultimate Membrane for Gas Separation. *Nano letters* **2009**, *9*, 4019-4024.

(27) Suk, M. E.; Aluru, N. R., Water Transport through Ultrathin Graphene. *The Journal of Physical Chemistry Letters* **2010**, *1*, 1590-1594.

(28) Su, J.; Zhao, Y.; Fang, C., Understanding the Role of Pore Size Homogeneity in the Water Transport through Graphene Layers. *Nanotechnology* **2018**, *29*, 225706.

(29) Heiranian, M.; Aluru, N. R., Nanofluidic Transport Theory with Enhancement Factors Approaching One. *ACS nano* **2020**, *14*, 272-281.

(30) Si, W.; Zhang, Y.; Sha, J.; Chen, Y., Mechanisms of Pressure-Induced Water Infiltration Process through Graphene Nanopores. *Molecular Simulation* **2019**, *45*, 518-524.

(31) Yan, Y.; Li, W.; Kral, P., Enantioselective Molecular Transport in Multilayer Graphene Nanopores. *Nano letters* **2017**, *17*, 6742-6746.

(32) Köhler, M. H.; Gavazzoni, C., Water Freezing in Mos2 Nanotubes. *The Journal of Physical Chemistry C* **2019**, *123*, 13968−13975.

(33) Plimpton, S., Fast Parallel Algorithms for Short-Range Molecular Dynamics. *Journal of Computational Physics* **1995**, *117*, 1-19.

(34) Zhou, W.; Wei, M.; Zhang, X.; Xu, F.; Wang, Y., Fast Desalination by Multilayered Covalent Organic Framework (Cof) Nanosheets. *ACS Appl Mater Interfaces* **2019**, *11*, 16847-16854.

(35) K., V. P.; Kannam, S. K.; Hartkamp, R.; Sathian, S. P., Water Desalination Using Graphene Nanopores: Influence of the Water Models Used in Simulations. *Phys Chem Chem Phys* **2018**, *20*, 16005-16011.

(36) Jiao, S.; Xu, Z., Non-Continuum Intercalated Water Diffusion Explains Fast Permeation through Graphene Oxide Membranes. *ACS nano* **2017**, *11*, 11152-11161.

(37) Ryckaert, J. P.; Ciccotti, G.; Berendsen, H. J. C., Numerical Integration of the Cartesian Equations of Motion of a System with Constraints: Molecular Dynamics of N-Alkanes. *Journal of Computational Physics* **1977**, *23*, 327.

(38) Werder, T.; Walther, J. H.; Jaffe, R. L.; Halicioglu, T.; Koumoutsakos, P., On the Water-Carbon Interaction for Use in Molecular Dynamics Simulations of Graphite and Carbon Nanotubes. *J. Phys. Chem. B* **2003**, *107*, 1345-1352.

(39) Wang, Y.; Wang, C.; Zhang, Y.; Huo, F.; He, H.; Zhang, S., Molecular Insights into the Regulatable Interfacial Property and Flow Behavior of Confined Ionic Liquids in Graphene Nanochannels. *Small* **2019**, *15*, 1804508.

(40) Falk, K.; Sedlmeier, F.; Joly, L.; Netz, R. R.; Bocquet, L., Molecular Origin of Fast Water Transport in Carbon Nanotube Membranes: Superlubricity Versus Curvature Dependent Friction. *Nano Letter* **2010**, *10*, 4067-73.

(41) Pascal, T. A.; Goddard, W. A.; Jung, Y., Entropy and the Driving Force for the Filling of Carbon Nanotubes with Water. *Proceedings of the National Academy of Sciences of the United States of America* **2011**, *108*, 11794-8.

(42) Farimani, A. B.; Aluru, N. R., Spatial Diffusion of Water in Carbon Nanotubes: From Fickian to Ballistic Motion. *J Phys Chem B* **2011**, *115*, 12145-9.

(43) Zheng, Y. G.; Ye, H. F.; Zhang, Z. Q.; Zhang, H. W., Water Diffusion inside Carbon Nanotubes: Mutual Effects of Surface and Confinement. *Phys Chem Chem Phys* **2012**, *14*, 964-71.

(44) Cao, W.; Huang, L.; Ma, M.; Lu, L.; Lu, X., Water in Narrow Carbon Nanotubes: Roughness Promoted Diffusion Transition. *The Journal of Physical Chemistry C* **2018**, *122*, 19124-19132.

(45) Hong, Y.; Zhang, J.; Zhu, C.; Zeng, X. C.; Francisco, J. S., Water Desalination through Rim Functionalized Carbon Nanotubes. *Journal of Materials Chemistry A* **2019**, *7*, 3583-3591.

(46) Park, S.; Schulten, K., Calculating Potentials of Mean Force from Steered Molecular Dynamics Simulations. *The Journal of chemical physics* **2004**, *120*, 5946-61.

(47) Grossfield, A., *Wham: The Weighted Histogram Analysis Method*, http://membrane.urmc.rochester.edu/content/wham, accessed March, 2018.

(48) Shen, C.; Guo, W., Manipulation of Long-Range Water Ordering in Less Confined Nanotubes. *The Journal of Physical Chemistry C* **2019**, *123*, 10101-10106.

(49) Gorshunov, B. P., et al., Incipient Ferroelectricity of Water Molecules Confined to Nano-Channels of Beryl. *Nat Commun* **2016**, *7*, 12842.

(50) Gorshunov, B. P.; Zhukova, E. S.; Torgashev, V. I.; Lebedev, V. V.; Shakurov, G. S.; Kremer, R. K.; Pestrjakov, E. V.; Thomas, V. G.; Fursenko, D. A.; Dressel, M., Quantum Behavior of Water Molecules Confined to Nanocavities in Gemstones. *J Phys Chem Lett* **2013**, *4*, 2015-20.

(51) Zhang, Z.; Li, X.; Yin, J.; Xu, Y.; Fei, W.; Xue, M.; Wang, Q.; Zhou, J.; Guo, W., Emerging Hydrovoltaic Technology. *Nature nanotechnology* **2018**, *13*, 1109-1119.

(52) Piegl, L. A.; Tiller, W., *The Nurbs Book*, 1995.

(53) Moulod, M.; Hwang, G., Water Self-Diffusivity Confined in Graphene Nanogap Using Molecular Dynamics Simulations. *J Appl Phys* **2016**, *120*, 194302.

(54) Köhler, M. H.; da Silva, L. B., Size Effects and the Role of Density on the Viscosity of Water Confined in Carbon Nanotubes. *Chemical Physics Letters* **2016**, *645*, 38-41.

(55) Won, C. Y.; Joseph, S.; Aluru, N. R., Effect of Quantum Partial Charges on the Structure and Dynamics of Water in Single-Walled Carbon Nanotubes. *The Journal of chemical physics* **2006**, *125*, 114701.

(56) Chiavazzo, E.; Fasano, M.; Asinari, P.; Decuzzi, P., Scaling Behaviour for the Water Transport in Nanoconfined Geometries. *Nat Commun* **2014**, *5*, 4565.

(57) Bocquet, L.; Barrat, J.-L., Hydrodynamic Boundary Conditions, Correlation Functions, and Kubo Relations for Confined Fluids. *Physical Review E* **1994**, *49*, 3079-3092.

(58) Xiong, W.; Liu, J. Z.; Ma, M.; Xu, Z.; Sheridan, J.; Zheng, Q., Strain Engineering Water Transport in Graphene Nanochannels. *Physical review. E, Statistical, nonlinear, and soft matter physics* **2011**, *84*, 056329.

(59) Luzar, A.; Chandler, D., Effect of Environment on Hydrogen Bond Dynamics in Liquid Water. *Physical review letters* **1996**, *76*, 928-931.

(60) Kohler, M. H.; Bordin, J. R.; da Silva, L. B.; Barbosa, M. C., Breakdown of the Stokes-Einstein Water Transport through Narrow Hydrophobic Nanotubes. *Phys Chem Chem Phys* **2017**, *19*, 12921-12927.

(61) Wang, Y.; Huo, F.; He, H.; Zhang, S., The Confined [Bmim][Bf4] Ionic Liquid Flow through Graphene Oxide Nanochannels: A Molecular Dynamics Study. *Phys Chem Chem Phys* **2018**, *20*, 17773-17780.

(62) Wu, K.; Chen, Z.; Li, J.; Li, X.; Xu, J.; Dong, X., Wettability Effect on Nanoconfined Water Flow. *Proceedings of the National Academy of Sciences* **2017**, *114*, 3358-3363.

(63) Cicero, G.; Grossman, J. C.; Schwegler, E.; Gygi, F.; Galli, G., Water Confined in Nanotubes and between Graphene Sheets: A First Principle Study. *Journal of the American Chemical Society* **2008**, *130*, 1871-8.

(64) Thomas, J. A.; McGaughey, A. J. H., Reassessing Fast Water Transport through Carbon Nanotubes. *Nano letters* **2008**, *8*, 2788-2793.

(65) Yongli, S.; Minhua, S.; Weidong, C.; Congxiao, M.; Fang, L., The Examination of Water Potentials by Simulating Viscosity. *Computational Materials Science* **2007**, *38*, 737-740.

(66) Yun, Y.; Khaliullin, R. Z.; Jung, Y., Low-Dimensional Confined Ice Has the Electronic Signature of Liquid Water. *J Phys Chem Lett* **2019**, *10*, 2008-2016.

(67) Alfè, D.; Gillan, M. J., First-Principles Calculation of Transport Coefficients. *Physical review letters* **1998**, *81*, 5161-5164.

(68) Sam, A.; K, V. P.; Sathian, S. P., Water Flow in Carbon Nanotubes: The Role of Tube Chirality. *Phys Chem Chem Phys* **2019**, *21*, 6566-6573.

(69) Lu, H.; Li, J.; Gong, X.; Wan, R.; Zeng, L.; Fang, H., Water Permeation and Wavelike Density Distributions inside Narrow Nanochannels. *Physical Review B* **2008**, *77*, 174115.

(70) Willems, K.; Ruic, D.; Biesemans, A.; Galenkamp, N. S.; Van Dorpe, P.; Maglia, G., Engineering and Modeling the Electrophoretic Trapping of a Single Protein inside a Nanopore. *ACS nano* **2019**, *13*, 9980−9992.

(71) Wang, F.-C.; Zhao, Y.-P., Slip Boundary Conditions Based on Molecular Kinetic Theory: The Critical Shear Stress and the Energy Dissipation at the Liquid–Solid Interface. *Soft Matter* **2011**, *7*, 8628.

(72) Yang, X.; Yang, X.; Liu, S., Molecular Dynamics Simulation of Water Transport through Graphene-Based Nanopores: Flow Behavior and Structure Characteristics. *Chinese Journal of Chemical Engineering* **2015**, *23*, 1587-1592.

(73) Thomas, J. A.; McGaughey, A. J., Water Flow in Carbon Nanotubes: Transition to Subcontinuum Transport. *Physical review letters* **2009**, *102*, 184502.

(74) Qin, X.; Yuan, Q.; Zhao, Y.; Xie, S.; Liu, Z., Measurement of the Rate of Water Translocation through Carbon Nanotubes. *Nano letters* **2011**, *11*, 2173-7.

(75) Kannam, S. K.; Todd, B. D.; Hansen, J. S.; Daivis, P. J., How Fast Does Water Flow in Carbon Nanotubes? *The Journal of chemical physics* **2013**, *138*, 094701.

TOC Graphic

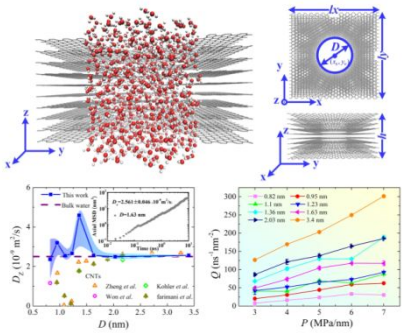
This work
Bulk water
CNTs
Zheng et al.
Kohler et al.
Won et al.
Tarimani et al.
D (nm)
P (MPa/nm)

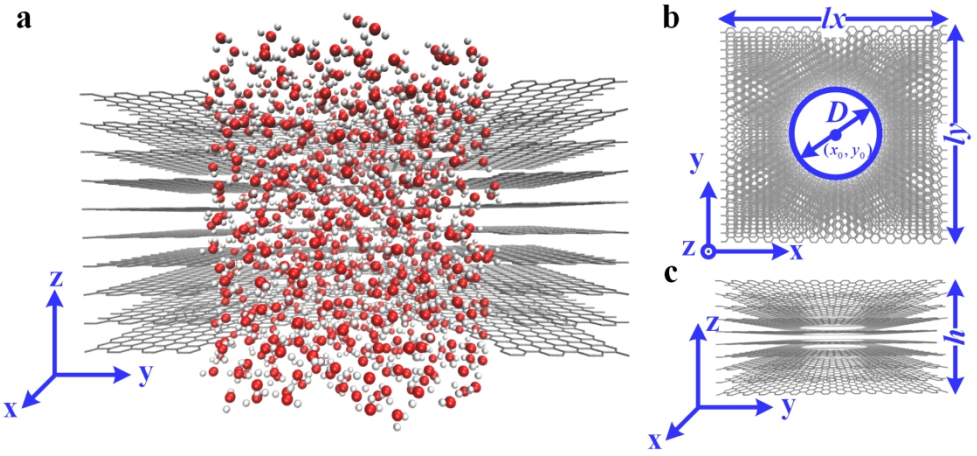


Figure 1. Representative atomic models of nanoconfined water in MGPNs (D = 3.4 nm). (a) Equilibrated nanoconfined water in MGPNs. The oxygen, hydrogen and carbon atoms were colored in red, white and gray, respectively. The MGPNs were constructed by overstacking of 10 graphene nanopores at a uniform distance of 0.34 nm. (b) and (c) were top and side views of the MGPNs. The orientation of the MGPNs were indicated by the coordinate system in each figure.

183x88mm (300 x 300 DPI)

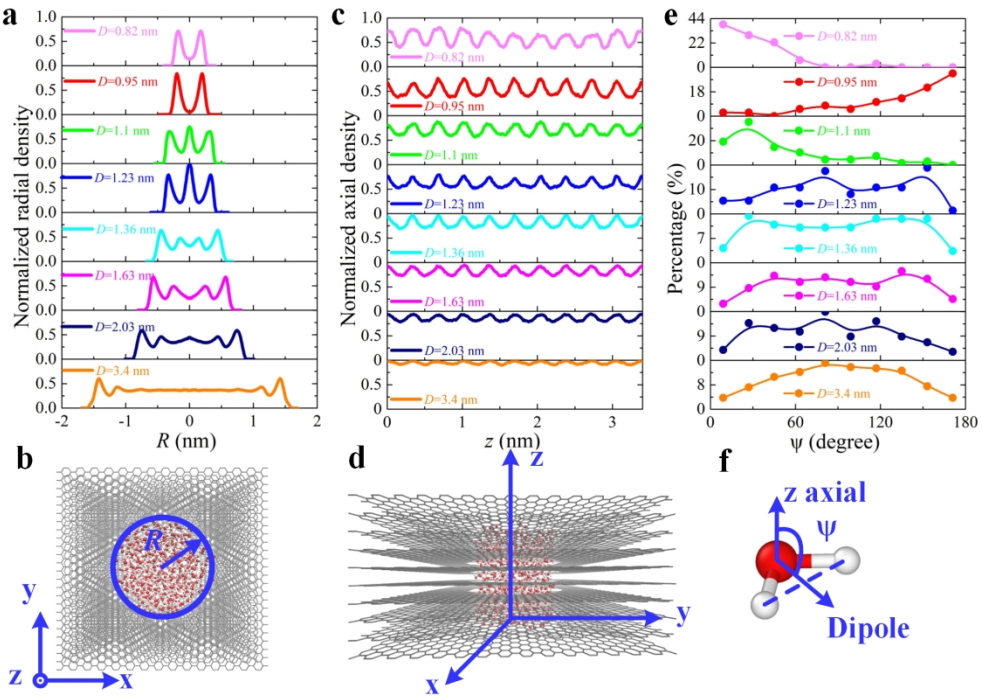


Figure 2. Water structure and dipole orientations in the MGPNs. All the water density profiles are normalized by the maximum values in each system (Here, 1.48295 g cm-3 for the radial density, 0.47902 g cm-3 for the axial density). (a-b) Radial density profile (RDP) in different MGPNs, and representative schematic of the radial density. (c-d) Axial density profile (ADP), and representative schematic of the axial density; (e-f) Water dipole orientation profile (DOP) in different MGPNs connected with B-Spline,52 and the definition of the water dipole orientation angle ψ.

186x136mm (300 x 300 DPI)

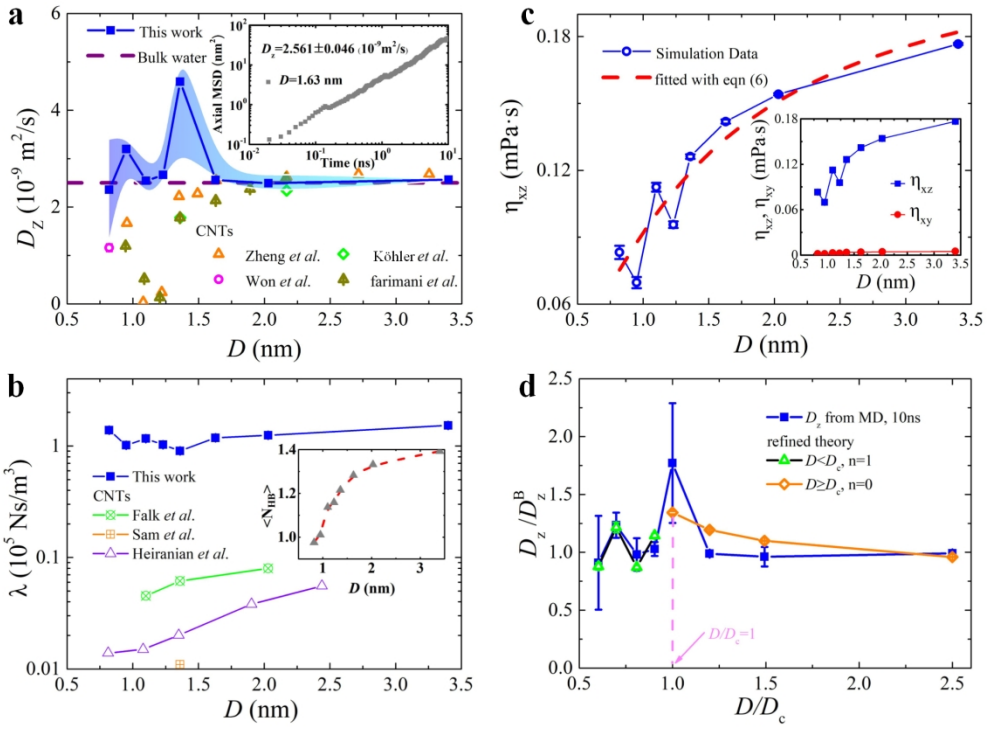


Figure 3. Nanoconfined water properties in MGPNs. (a) Axial diffusion coefficient Dz, with color strip represents errors by B-Splines.52 The inset shows the representative section of the mean squared displacement (MSD) used for calculating Dz, with more examples given in ESI Figures S6-S7. The diffusion coefficient of the bulk water DB Z= 2.59 × 10-9 m2 s-1 (purple dash line) is given for comparison.42 Previous reported water axial diffusion coefficient are shown with data adopted from Farimani et al.42, Zheng et al.43, Köhler et al.54, Won et al.55. (b) Friction coefficients of water molecules in different MGPNs. Former published results of water friction coefficient in CNTs are used for comparison, with data adopted from Falk et al.40, Sam et al.68 and Heiranian et al.29. The average numbers of HBs per water molecule in each MGPNs are shown as inset. (c) Axial shear viscosity of water ηxz in different MGPNs, with fitting model given in eq 6 as a red dash line. The inset shows axial (ηxz, blue dotted line) and radial (ηxy, red dotted line) water viscosities. (d) A refined model of Dz and its prediction, with data obtained at simulation time of 10 ns using eq 6.

185x138mm (300 x 300 DPI)

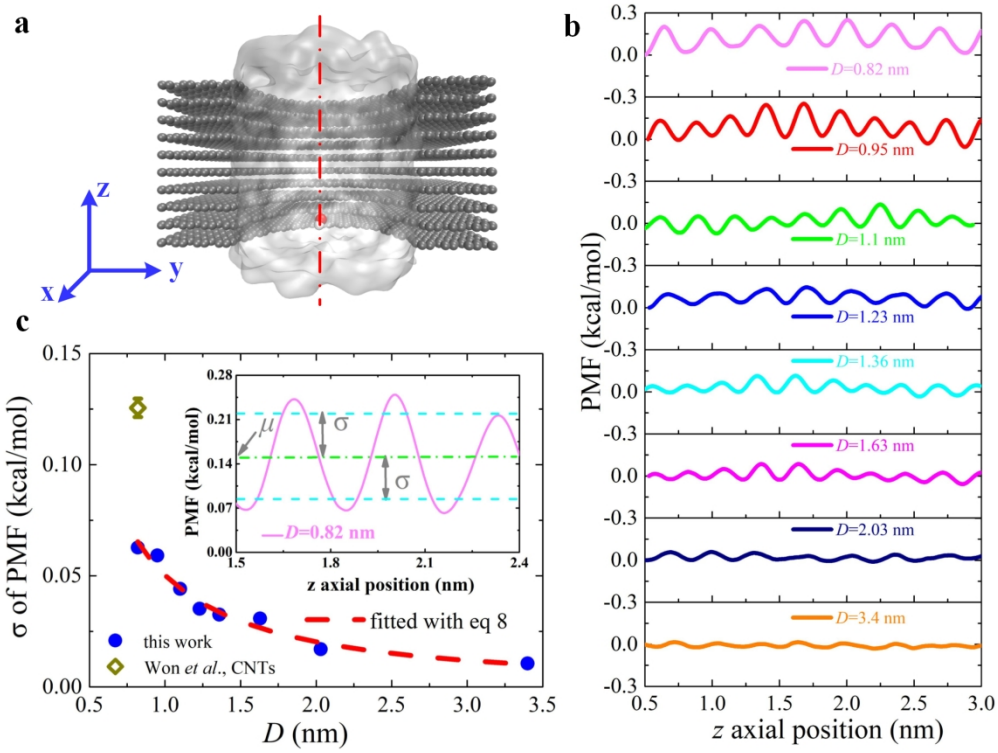


Figure 4. Potential of mean forces (PMFs) of a water molecule migrating through the MGPNs. (a) A typical system snapshot for calculating the PMFs with water migration path indicated by the axis (red dotted line) of the MGPNs. (b) The PMFs of water molecules migration in different MGPNs with their diameter D given as legends. (c) The standard deviation σ of water migration PMFs in MGPNs and CNTs. The results in this work were fitted with the proposed model given in eq 8. The σ value of water migration PMFs in CNTs for comparison was monitored in single-walled (6, 6) CNT.55 The inset illustrated the local fluctuation of the PMF.

190x144mm (300 x 300 DPI)

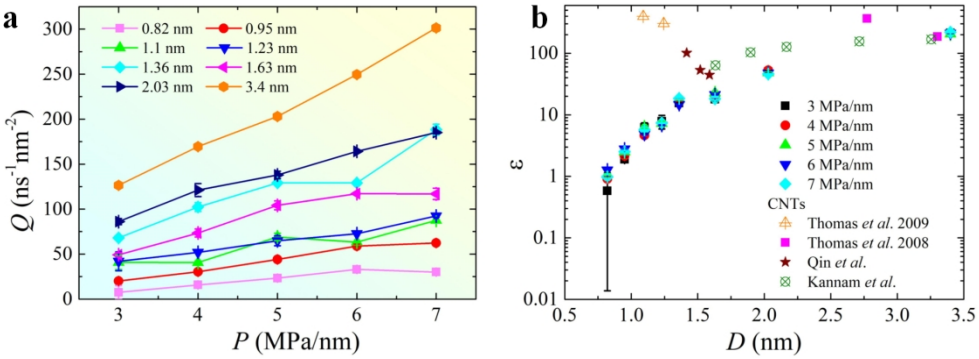


Figure 5. (a) Water flux Q vs. applied pressure gradient P in different MGPNs (the error of three independent MD simulations is within ±5%); (b) the flow enhancement factor ε against different diameters D using different gradients P (the error is within ±5%). Some other available results of the water confined in CNTs are also presented here, i.e. Thomas et al.73, Qin et al.74, Kannam et al.75

188x69mm (300 x 300 DPI)

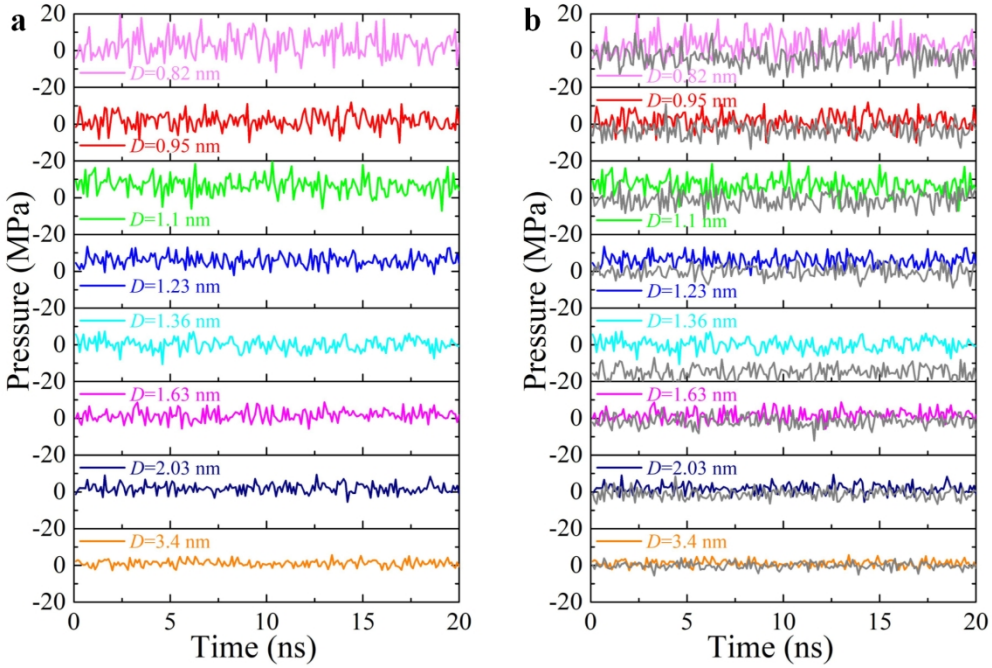


Figure S1. (a) Variations of the pressure with time during the last 20 ns equilibration MD simulations; (b) The pressure-time relation of our present MD systems and other systems with one less water molecule at the same nanopore diameter D during the last 20 ns equilibration MD simulations.

186x126mm (300 x 300 DPI)

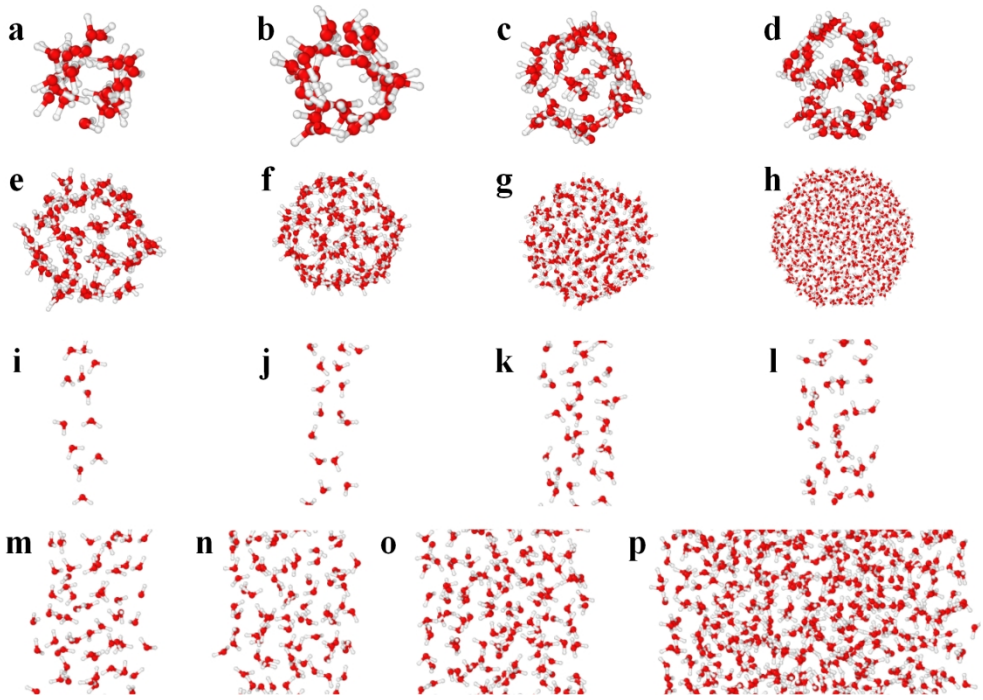


Figure S2. (a)-(h) Top view of water molecules confined in different MGPNs (D = 0.82, 0.95, 1.1, 1.23, 1.36, 1.63, 2.03, 3.4 nm); (i)-(p) Side view of water molecules.

178x124mm (300 x 300 DPI)

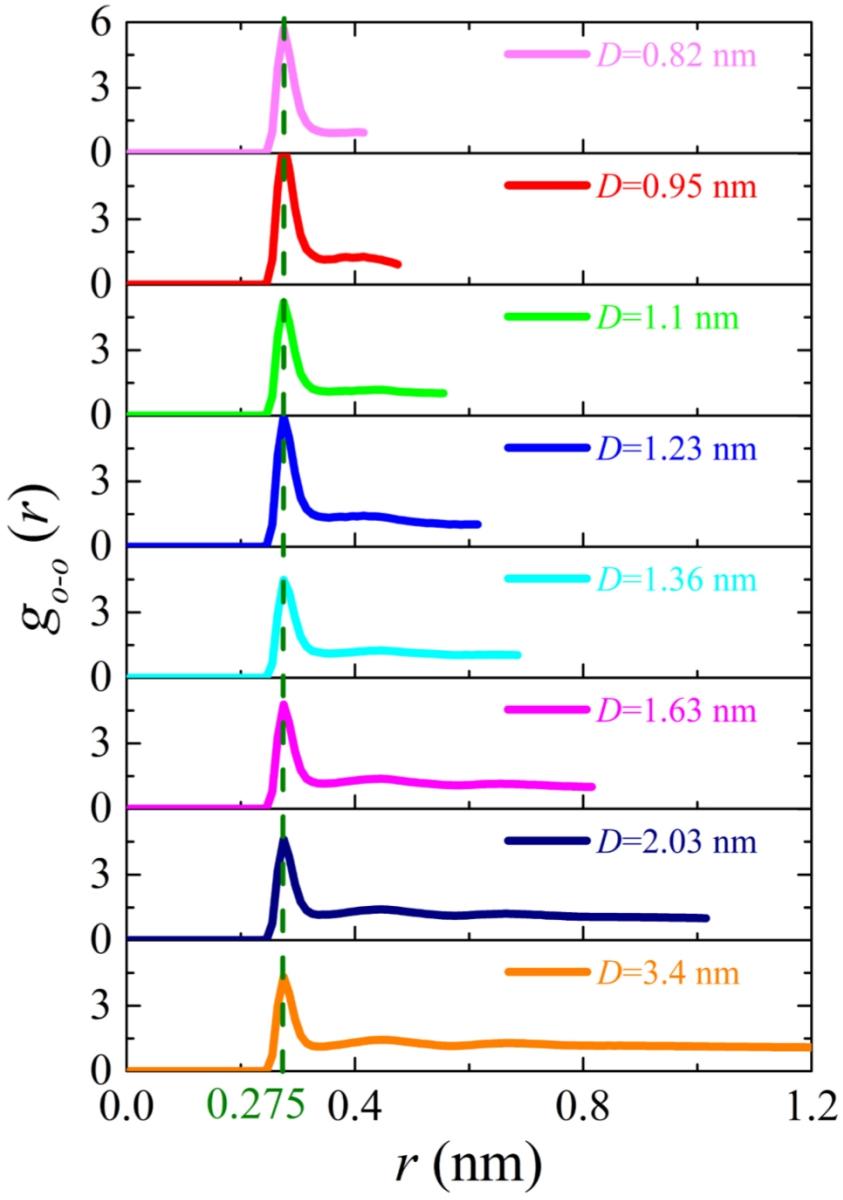


Figure S3. The Radial distribution function (RDF) using the Visual Molecular Dynamics (VMD)4. The position of the first peak in the RDF was r1 = 0.275 nm, which was used to determine the value of the effective molecular diameter a.3, 8 Here, the value of a was close to that in previous studies.5-6

92x131mm (300 x 300 DPI)

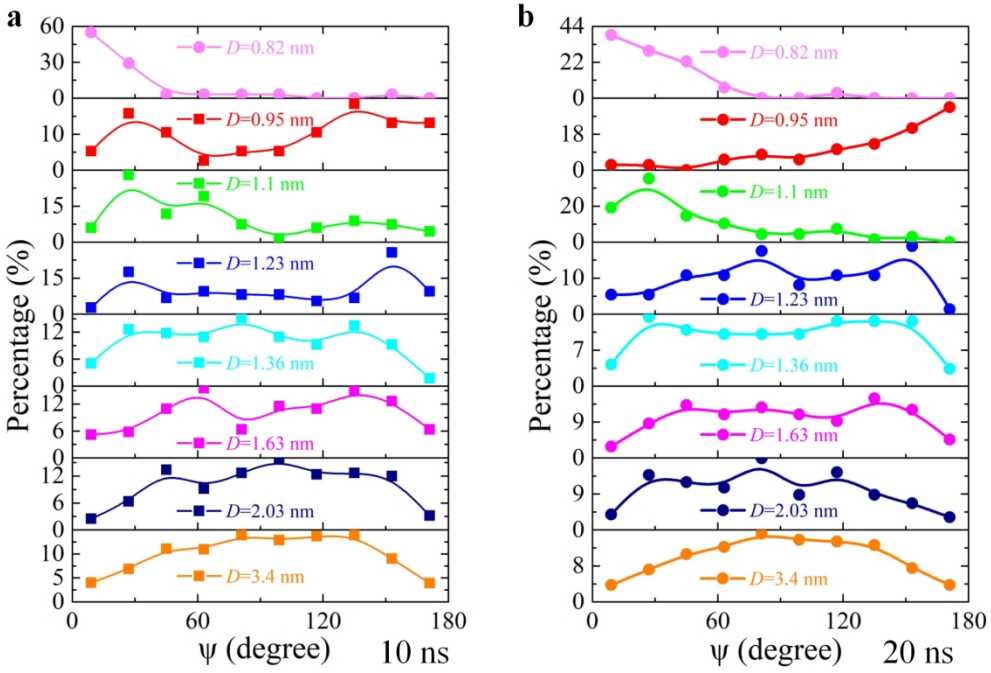


Figure S4. The DOP of two different MD simulation times, 10 ns (a), 20 ns (b). The values of the DOP were connected with B-Spline.9

189x132mm (300 x 300 DPI)

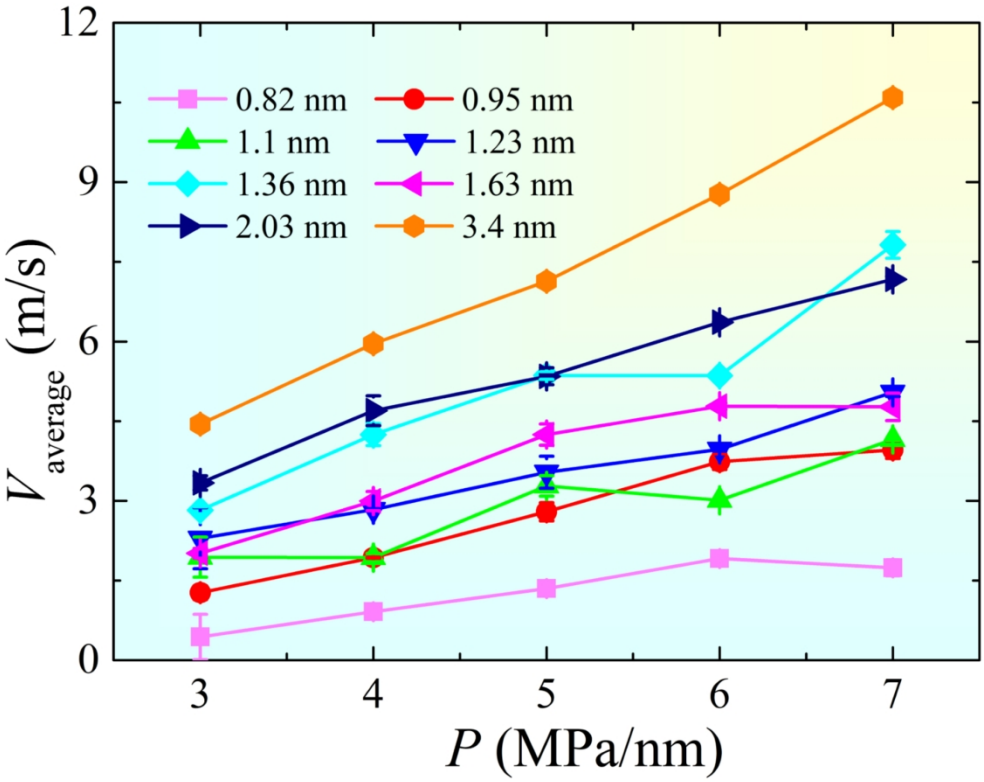


Figure S5. The average velocity Vaverage of water molecules confined in different MGPNs under five different pressure gradients P (P = 3, 4, 5, 6 and 7 MPa nm-1).

165x129mm (300 x 300 DPI)

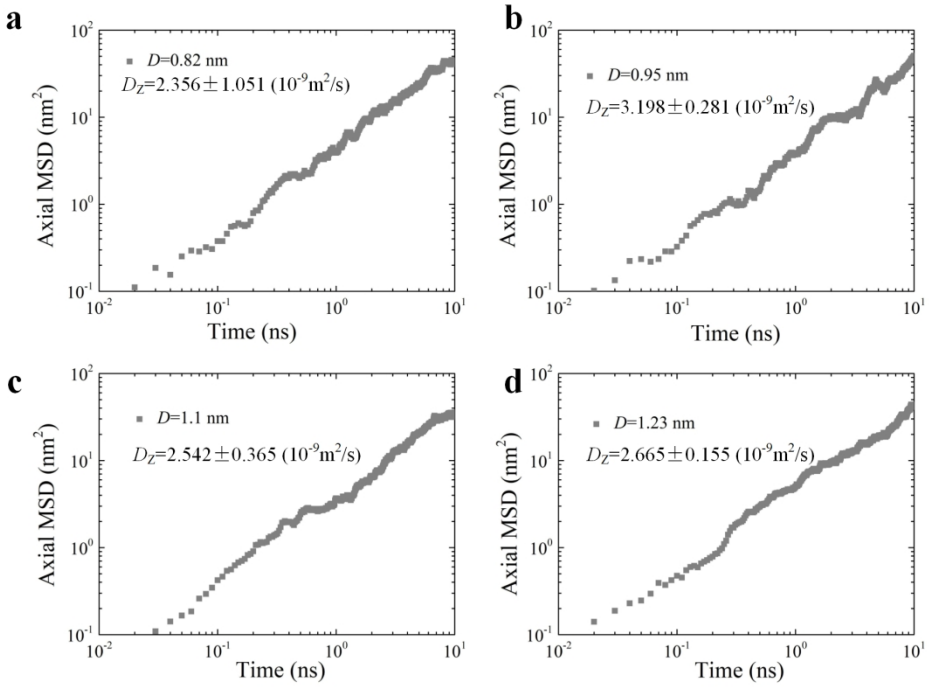


Figure S6. Logarithmic plot of the MSD of water molecules confined in different MGPNs (D = 0.82, 0.95, 1.1, 1.23 nm). The MD simulation time was 10 ns, similar to previous works10.

176x124mm (300 x 300 DPI)

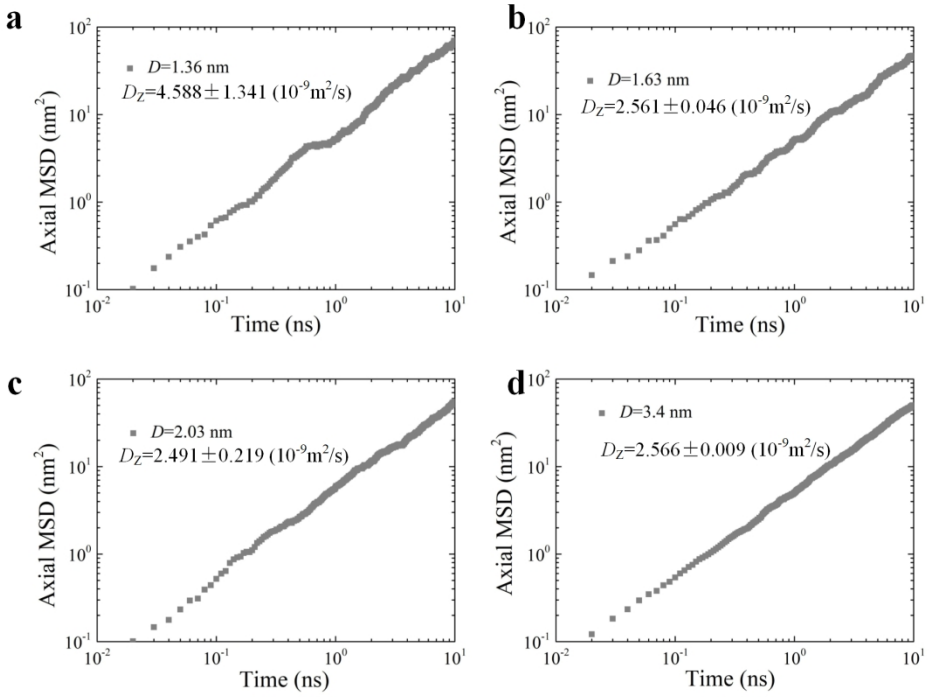


Figure S7. Logarithmic plot of the MSD of water molecules confined in different MGPNs D (D = 1.36, 1.63, 2.03, 3.4 nm). The MD simulation time was 10 ns, similar to previous works10.

175x125mm (300 x 300 DPI)

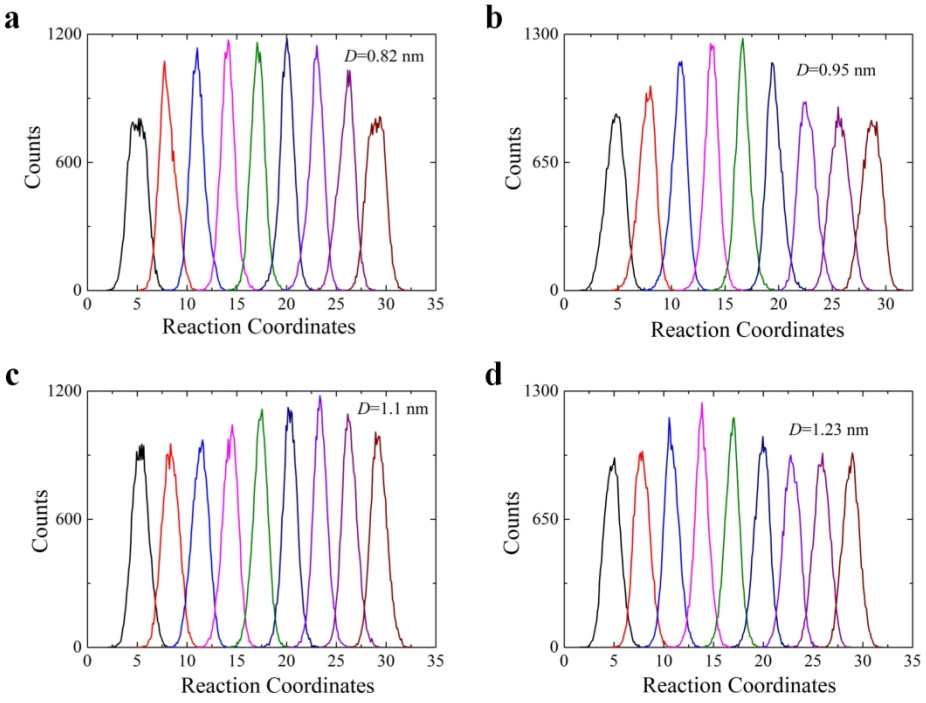


Figure S8. Histograms of configurations along reaction coordinates (D = 0.82, 0.95, 1.1, 1.23 nm)

182x130mm (300 x 300 DPI)

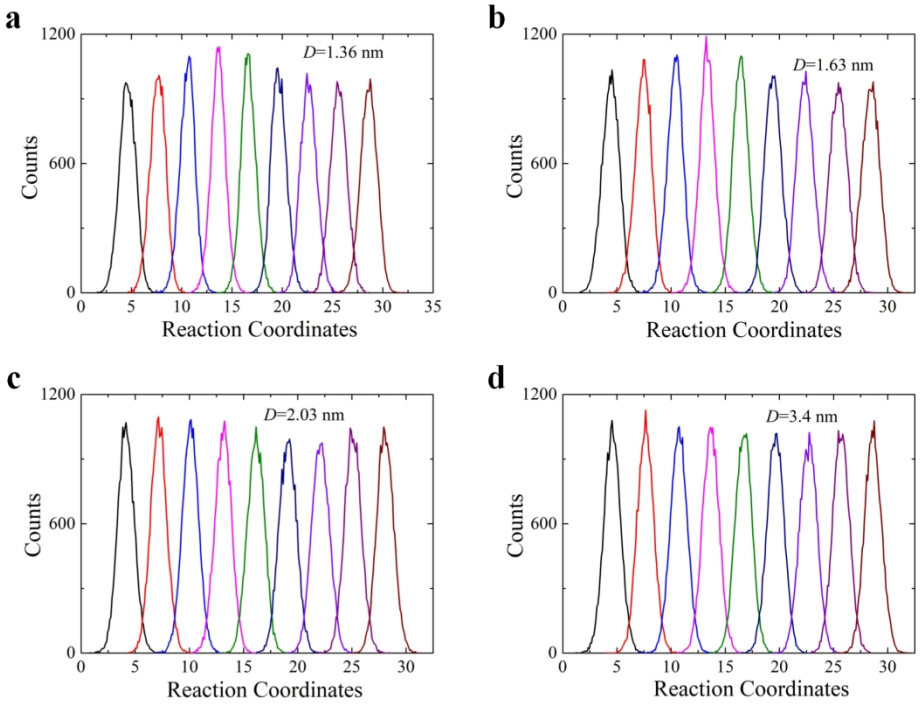


Figure S9. Histograms of configurations along reaction coordinates (D = 1.36, 1.63, 2.03, 3.4 nm)

182x131mm (300 x 300 DPI)